tures in the tropical atmosphere are water-like. Further examination of this point must rely on more spectral measurements, particularly in the near-infrared, where liquid water absorption and ice absorption become important.

REFERENCES AND NOTES

1. G. L. Stephens and S. Tsay, *Q. J. R. Meteorol. Soc.* **116**, 671 (1990).
2. R. D. Cess *et al.*, *Science* **267**, 496 (1995).
3. V. Ramanathan *et al.*, *ibid.*, p. 499.
4. F. P. J. Valero *et al.*, *Geophys. Res. Lett.* **10**, 1184 (1983); F. P. J. Valero *et al.*, *ibid.* **11**, 465 (1984).
5. The BBHFOV covered the entire hemisphere. Response time was 1 ms. The BBHFOV was calibrated versus a cavity radiometer, resulting in an absolute accuracy of 1%. The TDDR also had a hemispheric field of view but had seven discrete, narrow bandwidth (10-nm) channels throughout the visible and near-infrared. When the TDDR "looked" in the zenith direction, an oscillating shadow arm blocked the direct downwelling solar flux once per cycle (30 s); this variation allowed measurement of both the diffuse and the direct components of solar flux. Our study focuses on the spectral flux capabilities of the TDDR and, in particular, spectral hemispherical reflectance obtained from a nadir-viewing TDDR.
6. J. S. Foote and F. Rawlins, *IAMAP 89, Fifth Scientific Assembly of the International Association of Meteorology and Atmospheric Physics, Brief Review Papers and Abstracts*, B. W. Riddaway, Ed. (31 July to 12 August 1989, University of Reading, Reading, United Kingdom).
7. Z. Q. Li *et al.*, *J. Climate* **6**, 317 (1993).
8. We used the LOWTRAN7 atmospheric transmission model to calculate solar transmission between the surface and 10 km.
9. This is directly related to the issue of cloud absorption versus cloudy-column absorption. We are assuming that, as a result of the diffuse scattering by clouds, the strong water vapor bands are already saturated in the 10- to 20-km column such that the lower 10 km will not add appreciably to the total column absorption. Of course, this effect will depend on cloud thickness and geometry and potential absorbing aerosols in the lower troposphere.

10. This research was supported under NASA program code 460-42 and NSF grant 9223467.

31 October 1994; accepted 17 January 1995

Self-Assembled Metal Colloid Monolayers: An Approach to SERS Substrates

R. Griffith Freeman, Katherine C. Grabar, Keith J. Allison, Robin M. Bright, Jennifer A. Davis, Andrea P. Guthrie, Michael B. Hommer, Michael A. Jackson, Patrick C. Smith, Daniel G. Walter, Michael J. Natan*

The self-assembly of monodisperse gold and silver colloid particles into monolayers on polymer-coated substrates yields macroscopic surfaces that are highly active for surface-enhanced Raman scattering (SERS). Particles are bound to the substrate through multiple bonds between the colloidal metal and functional groups on the polymer such as cyanide (CN), amine (NH_2), and thiol (SH). Surface evolution, which can be followed in real time by ultraviolet-visible spectroscopy and SERS, can be controlled to yield high reproducibility on both the nanometer and the centimeter scales. On conducting substrates, colloid monolayers are electrochemically addressable and behave like a collection of closely spaced microelectrodes. These favorable properties and the ease of monolayer construction suggest a widespread use for metal colloid–based substrates.

In SERS, millionfold enhancements in Raman scattering can be obtained for molecules that are adsorbed at suitably rough surfaces of Au, Ag, and Cu (*1*). Although many approaches have been reported (*2*), preparation of well-defined, stable SERS substrates having uniform roughness on the critical scale of 3 to 100 nm has proven difficult. Because colloidal Au can be synthesized as monodisperse solutions throughout most of this size regime (*3*) and because molecules adsorbed to closely spaced, colloidal Au and Ag exhibit enhanced Raman scattering (*4*), these particles are excellent building blocks for SERS-active substrates.

The key issue is whether colloidal Au and Ag particles can be organized into macroscopic surfaces that have a well-defined and uniform nanometer-scale architecture. Indeed, controlling nanostructure is currently a central focus throughout materials research (*5*). Progress in the self-assembly of organic thin films on metal surfaces (*6*) led us to explore the reverse process: the self-assembly of colloidal Au and Ag particles onto supported organic films. As detailed below, this approach has yielded surfaces that are SERS-active, characterizable at both the macroscopic and the microscopic levels, highly reproducible, electrochemically addressable, and simple to prepare in large numbers. Moreover, these substrates have a surface roughness that is defined by the colloid diameter (which is tunable) and an average interparticle spacing that is continuously variable. As such, self-assembled Au and Ag colloid monolayers are likely to have extraordinary utility for SERS.

Our construction protocol for SERS-active Au and Ag colloid monolayers exploits the simplicity of self-assembly from solution and the affinity of noble metal surfaces for certain organic functional groups (Fig. 1). In our case, these moieties are present by virtue of organic films either polymerized or deposited on the surface of macroscopic (≈0.8 cm by 2 cm) substrates. Immersion of the functionalized substrate into a dilute solution of monodisperse colloidal Au or Ag particles leads to colloid immobilization. This solution-based process is extremely general, encompassing numerous permutations of insulating and conducting substrates (glass, quartz, plasma-treated Teflon, Formvar, indium-doped SnO_2, and Pt), organic films [hydrolyzed mono-, di-, and trialkoxysilanes containing the functional groups CN, NH_2, 2-pyridyl, $P(C_6H_5)_2$, and SH, as well as carboxyl-terminated C_{18} organothiol self-assembled monolayers], and colloids (5 to 70 nm in diameter for Au and 5 to 20 nm in diameter for Ag and Au-Ag composites) (*7*, *8*).

Solution-based surface assembly also eliminates preparative, geometric, and operational constraints associated with most previously described SERS substrates (*1*, *2*). Thus, 1 liter of 17 nM, 12-nm-diameter colloidal Au, which can be stored indefintely at room temperature, can be used to prepare 2000 0.5-cm^2 surfaces with only a 1% decrease in colloid concentration. Importantly, these substrates can be assembled sequentially or simultaneously. Surfaces in novel geometries that extend the utility of SERS can now be derivatized, including one face of a 5-μl spectroelectrochemical cell, large glass sheets several centimeters on a side, and the inside of a glass capillary with an inner diameter of 20 μm (*8*). Moreover, once constructed, no further activation steps (such as electrochemical oxidation-reduction cy-

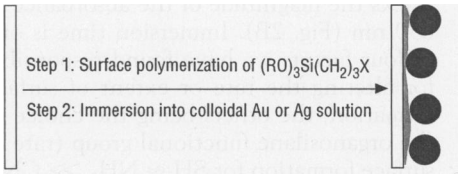

Fig. 1. Assembly strategy for Au and Ag colloid monolayers; X = CN, NH_2, 2-pyridyl, $P(C_6H_5)_2$, or SH; R = CH_3 or CH_2CH_3.

R. G. Freeman, Division of Science, Northeast Missouri State University, Kirksville, MO 63501, USA.
K. C. Grabar, K. J. Allison, R. M. Bright, J. A. Davis, A. P. Guthrie, M. B. Hommer, M. A. Jackson, P. C. Smith, D. G. Walter, M. J. Natan, Department of Chemistry, The Pennsylvania State University, 152 Davey Laboratory, University Park, PA 16802, USA.

*To whom correspondence should be addressed.

Downloaded from www.sciencemag.org on May 3, 2012

cles or particle aggregation) are required to initiate SERS activity.

Two lines of evidence demonstrate that immobilized particles are located solely at the surface of, and are not embedded within, the organic film. (i) Colloidal particles are very tightly attached to the polymer (when stored in water, no particle dissociation occurs after 1 year), yet monolayer formation does not occur on polymers with pendant methyl or methoxy groups. These data indicate that multiple specific covalent interactions between polymer functional groups (which are oriented toward the solution) and the particle surface are necessary for immobilization. (ii) Although SERS spectra for adsorbates from solution are easily obtained (see below), the SERS spectra of organosilane polymer films underneath Au monolayers are quite weak. This result contrasts with the results of SERS studies of colloid-polymer mixtures (*9*) and demonstrates that the surface of immobilized metal particles is accessible to solvent. In accord with this finding is our observation that the optical spectrum of Au colloid monolayers on transparent substrates depends on the dielectric constant of the surrounding medium (*7*).

The optical properties of colloidal Au and the nature of self-assembly offer an unprecedented opportunity to monitor surface evolution in real time. The time course of the formation of a Au colloid monolayer on a glass slide coated with polymerized 3-aminopropyltrimethoxysilane (APTMS) is shown in Fig. 2A. Binding of 12-nm-diameter Au particles to amine groups on the surface is indicated by an absorbance feature at 520 nm, the location of the Mie resonance for isolated small Au particles (*10*). As the particle coverage increases, interparticle spacing becomes small compared to the incident wavelength, and a new feature corresponding to a collective particle surface plasmon oscillation grows in at ~650 nm. This feature is responsible for the pronounced SERS activity of collections of colloidal Au particles (*4*). Accordingly, when a colloid monolayer in various stages of formation is placed in a solution containing the adsorbate *trans*-1,2-bis(4-pyridyl)ethylene (BPE), the SERS intensity for the ring stretch at 1610 cm^{-1} closely tracks the magnitude of the absorbance at 650 nm (Fig. 2B). Immersion time is one of four factors we have found responsible for altering the rate or extent of surface formation, the others being the choice of the organosilane functional group (rate of surface formation for SH ≈ NH_2 ≫ CN), the colloid concentration, and the presence or absence of an adsorbate on the colloidal particle.

This high degree of control over surface formation has important ramifications for reproducibility, a long-standing complication in SERS research (*1*). For example, when BPE was adsorbed to eight identical Ag colloid monolayers on glass, the greatest variation in integrated peak intensity for the 1610 cm^{-1} band was less than 8%. Similarly, for five different locations on a single substrate, the greatest difference was only 5%. As these values incorporate intrinsic errors associated with variation in laser power and sample positioning, the actual sample reproducibility is significantly better (*11*). This reproducibility extends to the nanometer scale, where Au and Ag colloid monolayers have been imaged by transmission electron microscopy (TEM), field-emission scanning electron microscopy (FE-SEM), and atomic force microscopy (AFM). A representative TEM image of an Au colloid monolayer prepared on an SiO_x-coated Formvar surface is shown in Fig. 3A. The Au particles are confined to a single layer, and the vast majority of particles are isolated from each other, unlike earlier systems of SERS-active Au and Ag colloids studied by TEM (*12*). Furthermore, the large field of view available with TEM allows us to conclude that particle aggregation has been eliminated over the entire sample. Similar conclusions obtain from large-field FE-SEM images and from multisite tapping-mode AFM images of Au-modified glass surfaces (*13*). We have demonstrated that the spacing obtained on these colloid-based surfaces is sufficient to yield SERS enhancement. Figure 3B shows the SERS spectrum of BPE adsorbed onto the derivatized TEM grid pictured in Fig. 3A.

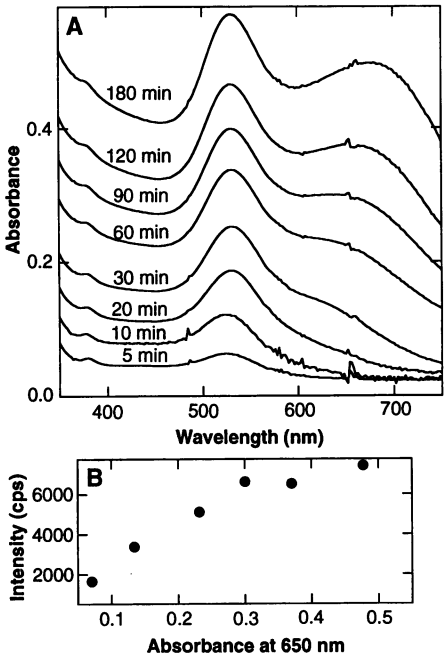

Fig. 2. Kinetics of the formation of Au colloid monolayers as measured by ultraviolet-visible (UV-VIS) spectroscopy and SERS. (**A**) A series of UV-VIS spectra of Au colloid-functionalized glass slides in H_2O obtained with a Hewlett-Packard 8452A spectrophotometer. Cleaned (4:1 H_2SO_4:H_2O_2, 70°C) rectangular glass slides (~0.9 mm by 25 mm) were placed into a dilute solution of APTMS [0.3 ml of APTMS in 3 ml of methanol (CH_3OH)] for 12 hours and rinsed with CH_3OH upon removal. The polymer-coated slides were then immersed in a 17 nM solution of 12-nm-diameter colloidal Au particles (wavelength maximum = 520 nm) (*7, 22*). At each time indicated (and at several others not shown), the slide was removed from the Au colloid solution and an optical spectrum was recorded in H_2O, followed by a SERS spectrum in 4 mM BPE in 95:5 H_2O:CH_3OH (20 mW, 632.8 nm, Spex 1403 double monochromator, Hamamatsu R928 photomultiplier tube; band pass, 7 cm^{-1}; scan rate, 1 cm^{-1} s^{-1}; integration time, 1 s). (**B**) SERS intensity for the 1610-cm^{-1} band versus absorbance at 650 nm. Other bands in the BPE SERS spectrum evolve with identical kinetics.

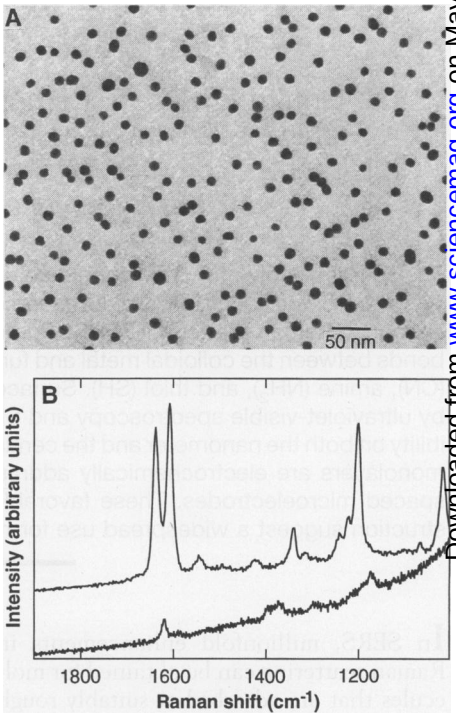

Fig. 3. (**A**) Image from a Formvar-coated Cu TEM grid that had been sputter-coated with a thin layer of SiO_x (Ted Pella, Inc.), treated for 2.5 hours in neat 3-cyanopropyldimethylmethoxysilane, rinsed exhaustively with CH_3OH upon removal, and immersed for 12 hours in colloidal Au (12 nm in diameter) (*7, 22*). Imaging was performed on a JEOL 1200 EXII instrument operated at an accelerating voltage of 80 kV. The area depicted is 0.28 μm^2 and is representative of the sample surface. (**B**) SERS spectrum (upper curve) of 5 μl of 1 mM BPE drop-coated onto the surface of the derivatized TEM grid (100 mW; 647.1 nm; band pass, 5 cm^{-1}; step, 2 cm^{-1}; integration time, 2 s). For comparison, an identical quantity of BPE was drop-coated onto an underivatized SiO_x grid; the Raman scattering from this sample is shown in the lower curve (step, 1 cm^{-1}; integration time, 1 s).

Downloaded from www.sciencemag.org on May 3, 2012

For comparison, the Raman scattering spectrum of an equivalent amount of BPE deposited onto an unmodified SiO_x-coated TEM grid is also shown in Fig. 3B. The intensity difference in these two samples clearly demonstrates the enhancing properties of colloid-based surfaces.

Another important feature of film-supported metal colloid monolayers is that the particles are subject to electrochemical potentials applied to underlying conductive substrates. Consequently, like SERS-active electrodes, Ag colloids immobilized on Pt exhibit an electrochemical potential-dependent SERS intensity for adsorbed pyridine (Fig. 4) (*14*). Identical maxima for the two surfaces in the plots of intensity versus potential suggests that the voltage drop across the polymer film is minimal. Voltammetry at colloid-based surfaces also resembles that at macroscopic electrodes. The first reduction wave for methyl viologen (MV^{2+}) is markedly rectified at an organosilane-coated Pt electrode (Fig. 4, inset) but returns upon immobilization of Au particles. The slightly broadened peak-to-peak separation is expected for an array of closely spaced microelectrodes (*15*). In view of the demonstrated biocompatibility of Au particles 5 to 20 nm in diameter (*3*), the ability to make electrochemical measurements at Au colloid monolayers suggests possible electrode-based biosensor applications (*16*).

Interparticle spacing in preformed Au monolayers can be further reduced by chemical deposition of a Ag coating; increased interparticle coupling because of decreased spacing and concomitant changes in dielectric properties lead to a dramatic increase in SERS activity. The optical and SERS spectra before and after deposition of Ag onto 18-nm-diameter colloidal Au are shown in Fig. 5. Initially, relatively large interparticle spacing is indicated by the absence of a collective particle surface plasmon band in the ultraviolet-visible and by a weakly enhanced SERS spectrum for adsorbed *p*-nitrosodimethylaniline (*p*-NDMA). Deposition of Ag causes a large increase in extinction at all wavelengths as well as a shift in the maximum wavelength λ_{max} from 520 to 386 nm. The shift in energy of and increased extinction at λ_{max} concur with expectations based on a computer algorithm for predicting the optical properties of isolated coated particles (*10*); the best agreement between the experimental and model data was reached with a 4-nm Ag coating (to make 26-nm-diameter particles) (*17*). The exceptional SERS activity (enhancement factor $\geq 10^5$) (*18*) of these substrates reflects optimization of the thickness of the Ag coating for this particular particle size and spacing of colloidal Au. Even greater enhancements may be possible with other combinations.

The Au and Ag colloid-based surfaces have many of the best attributes of previously described SERS substrates (uniform particle size, electrochemical addressability, and large enhancement factors) and a combination of other features that few surfaces can match (ease of characterization, no geometric constraints, low cost, and very high intra- and intersample reproducibility). These advantages, together with the ability to vary particle size, spacing, and the nature of the monolayer support, suggest a rich use for these materials in fundamental and applied studies. For example, as far as we know, no theoretical model correlating SERS activity with particle size or spacing (*19*) has been quantitatively tested; metal colloid monolayers should allow such experiments to be carried out. Most importantly, SERS can now be considered for applications in which the preparation of multiple high-quality substrates was previously viewed as an insurmountable barrier.

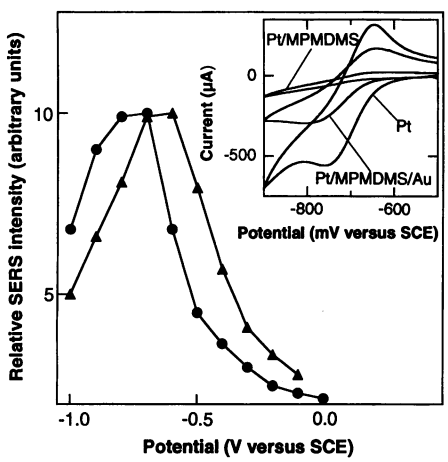

Fig. 4. Electrochemical potential dependence of the SERS intensity of the 1006 cm^{-1} band of pyridine on bulk Ag (▲) and on a Ag colloid monolayer on Pt (●) (*14*); SCE, saturated calomel electrode. The monolayer was prepared as follows: Clean Pt foil was placed into neat APTMS for 4 hours. After it was rinsed with triply distilled H_2O and air-dried, the polymer-coated foil was dipped in Ag colloid solution (*23*) for 1 hour. The derivatized foil was then rinsed with triply distilled H_2O and air-dried. In the absence of colloidal Ag, no pyridine SERS spectra were observed at any potential. See Fig. 2 for spectral acquisition parameters. **(Inset)** Cyclic voltammograms (100 mV s^{-1}, N_2 atmosphere) of 5 mM MV^{2+} in 0.1 M Na_2SO_4 on three surfaces: unmodified Pt, Pt coated with surface-polymerized 3-mercaptopropylmethyldimethoxysilane (MPMDMS), and Pt coated with MPMDMS and derivatized with 15-nm-diameter Au particles (5 hours in neat silane, rinsed, and then immersed for 4 hours in colloidal Au).

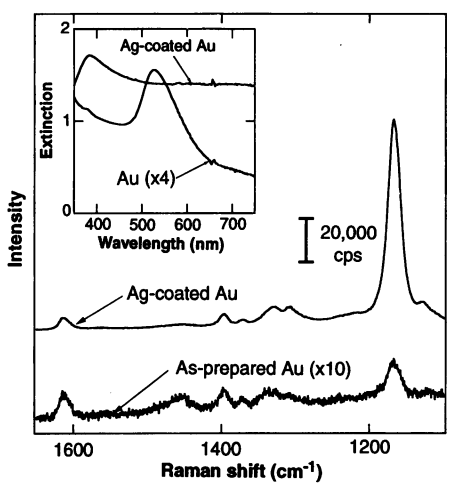

Fig. 5. Effect of Ag coating on the UV-VIS and SERS spectra of preformed Au colloid monolayers. The initial substrates were prepared as in Fig. 2, except that the organic film was formed from reaction with 2-(trimethoxysilyl)ethyl-2-pyridine (PETMS) for 24 hours. We carried out the Ag coating by immersing Au colloid monolayers into a 1:1 mixture of LI Silver enhancer and initiator solutions (Nanoprobes, Stony Brook, New York) for 13 min. The SERS spectra were of 0.5 mM *p*-NDMA solutions in CH_3OH. When Ag is deposited from the plating solution onto a PETMS-derived polymer on glass in the absence of colloidal Au, no SERS intensity could be observed for the same *p*-NDMA solution, irrespective of coating time. **(Inset)** Optical spectra were measured in H_2O. Instrumental parameters were as described in Fig. 2.

REFERENCES AND NOTES

1. For reviews, see: I. R. Nabiev, K. V. Sokolov, M. Manfait, in *Biomolecular Spectroscopy, Part A*, R. J. H. Clark and R. E. Hester, Eds. (Wiley, Chicester, England, 1993), vol. 20, chap. 7; J. J. Laserna, *Anal. Chim. Acta* **283**, 607 (1993); W. E. Smith, *Methods Enzymol.* **226**, 482 (1993); A. Otto, I. Mrozek, H. Grabhorn, W. Akemann, *J. Phys. Condens. Matter* **4**, 1143 (1992); R. L. Birke, T. Lu, J. R. Lombardi, in *Techniques for Characterization of Electrodes and Electrochemical Processes*, R. Varma and J. R. Selman, Eds. (Wiley, New York, 1991), chap. 5.
2. B. Pettinger, X. Bao, I. C. Wilcock, M. Muhler, G. Ertl, *Phys. Rev. Lett.* **72**, 1561 (1994); R. P. Van Duyne, J. C. Hulteen, D. A. Treichel, *J. Chem. Phys.* **99**, 2101 (1993); S. E. Roark and K. L. Rowlen, *Chem. Phys. Lett.* **212**, 50 (1993); P. A. Schueler *et al.*, *Anal. Chem.* **65**, 3177 (1993); K. I. Mullen and K. T. Carron, *ibid.* **63**, 2196 (1991); V. L. Schelgel and T. M. Cotton, *ibid.*, p. 241; P. Dawson, J. W. Haas III, K. B. Alexander, J. Thompson, T. L. Ferrell, *Surf. Sci. Lett.* **250**, L383 (1991); P. F. Liao and M. B. Stern, *Opt. Lett.* **7**, 483 (1982); S. Byahut and T. E. Furtak, *Langmuir* **7**, 508 (1991); R. L. Moody, T. Vo-Dinh, W. H. Fletcher, *Appl. Spectrosc.* **41**, 966 (1987); K. T. Carron, W. Fluhr, M. Meier, A. Wokaun, H. W. Lehmann, *J. Opt. Soc. Am. B* **3**, 430 (1986).
3. D. A. Handley, in *Colloidal Gold: Principles, Methods, and Applications*, M. A. Hayat, Ed. (Academic Press, San Diego, 1989), vols. 1 and 2.
4. J. Clarkson, C. Campbell, B. N. Rospendowski, W. E. Smith, *J. Raman Spectrosc.* **22**, 771 (1991); S. A. Soper, K. L. Ratzhlaff, T. Kuwana, *Anal. Chem.* **62**, 1438 (1990); D. Fornasiero and F. Grieser, *J. Chem. Phys.* **87**, 3213 (1987); X. K. Zhao and J. H. Fendler, *J. Phys. Chem.* **92**, 3350 (1988); J. A. Creighton, C. G. Blatchford, M. G. Albrecht, *Chem. Soc. Faraday Trans. 2* **75**, 790 (1979).

Downloaded from www.sciencemag.org on May 3, 2012

5. J. M. Schnur, *Science* **262**, 1669 (1993); C. A. Huber *et al.*, *ibid.* **263**, 800 (1994); G. M. Whitesides, J. P. Mathias, C. T. Seto, *ibid.* **254**, 1312 (1991).
6. C. D. Bain and G. M. Whitesides, *Angew. Chem. Int. Ed. Engl.* **28**, 506 (1989); A. Ulman, *An Introduction to Ultrathin Organic Films, from Langmuir-Blodgett to Self-Assembly* (Academic Press, Boston, 1991).
7. K. C. Grabar, R. G. Freeman, M. B. Hommer, M. J. Natan, *Anal. Chem.*, in press.
8. K. C. Grabar *et al.*, in preparation.
9. P. Matejka, B. Vlcková, J. Vohlidal, P. Pancoska, V. Baumruk, *J. Phys. Chem.* **96**, 1361 (1992); P. C. Lee and D. Meisel, *Chem. Phys. Lett.* **99**, 262 (1983).
10. C. Bohren and D. R. Huffman, *Absorption and Scattering of Light by Small Particles* (Wiley, New York, 1983).
11. K. C. Grabar *et al.*, in preparation.
12. P. X. Zhang, Y. Fang, W. N. Wang, D. H. Ni, S. Y. Fu, *J. Raman Spectrosc.* **21**, 127 (1990); J. Wiesner and A. Wokaun, *Chem. Phys. Lett.* **157**, 569 (1989); C. G. Blatchford, J. R. Campbell, J. A. Creighton, *Surf. Sci.* **120**, 435 (1982).
13. The AFM image from a glass slide coated with 3-aminopropylmethyldimethoxysilane indicates an overall roughness of 1 to 3 nm, notwithstanding a few isolated locations where the polymer roughness approaches 8 to 10 nm. This roughness scale is typical for organosilane films on glass or quartz (*20*). Immobilization of 12-nm colloidal Au particles to a coverage equivalent to that shown for 180 to 210 min in Fig. 2A yields a surface with features 12 to 20 nm high and 20 to 30 nm wide. The increased dispersion in particle size relative to TEM results from convolution of the true particle size with the AFM tip size (*21*) but is nevertheless of sufficient quality to indicate that the surface is composed of a monolayer of separated particles, in agreement with FE-SEM images on similar substrates.
14. D. L. Jeanmaire and R. P. Van Duyne, *J. Electroanal. Chem.* **84**, 1 (1977).
15. C. Amatore, J. M. Savéant, D. Tessier, *ibid.* **147**, 39 (1983).
16. A. E. G. Cass, Ed., *Biosensors: A Practical Approach* (Oxford Univ. Press, Oxford, 1990).
17. The optical constants for Au and Ag were taken from R. H. Morriss and L. F. Collins [*J. Chem. Phys.* **41**, 3357 (1961)]. These values were fit to exponential curves to generate continuous values between 300 and 700 nm.
18. We calculated an enhancement factor (EF) of 5.7×10^5 for the Ag-coated surface by comparing the ratios of background-corrected intensities for a SERS spectrum and a solution spectrum in units of counts per second per watt per molecule, and averaging the EF values obtained for six different common peaks. A low signal-to-noise ratio precluded calculation of accurate EFs for the as-prepared Au sample.
19. E. J. Zeman and G. C. Schatz, *J. Phys. Chem.* **91**, 634 (1987); M. Inoue and K. Ohtaka, *J. Phys. Soc. Jpn.* **52**, 3853 (1983); L.-C. Chu and S.-Y. Wang, *J. Appl. Phys.* **57**, 453 (1985); *Phys. Rev. B* **31**, 693 (1985).
20. S. Karrasch, M. Dolder, F. Schabert, J. Ramsden, A. Engel, *Biophys. J.* **65**, 2437 (1993); W. J. Dressick, C. S. Dulcey, J. H. Georger Jr., G. S. Calabrese, J. M. Calvert, *J. Electrochem. Soc.* **141**, 210 (1994).
21. D. Keller, *Surf. Sci.* **253**, 353 (1991).
22. G. Frens, *Nature Phys. Sci.* **241**, 20 (1973); W. S. Sutherland and J. D. Winefordner, *J. Colloid Interface Sci.* **48**, 129 (1992).
23. P. C. Lee and D. Meisel, *J. Phys. Chem.* **86**, 3391 (1982).
24. This research was supported in part by the Petroleum Research Fund (25694-G5) administered by the American Chemical Society, the Beckman Young Investigator Program, and The Pennsylvania State University (PSU). The National Science Foundation (CHE-9300292) provided an undergraduate fellowship to M.B.H., the Particulate Materials Center at PSU furnished an undergraduate fellowship to P.C.S., and Eastman Kodak Company underwrote for a graduate fellowship to K.C.G. We thank PPG Industries for a gift of SnO_2, the Electron Microscopy Facility for the Life Sciences in the Biotechnology Institute at PSU, and C. T. Bohren for the computer programs BHMIE and BHCOAT.

20 September 1994; accepted 29 December 1994

Granular Convection Observed by Magnetic Resonance Imaging

E. E. Ehrichs, H. M. Jaeger,* Greg S. Karczmar, James B. Knight, Vadim Yu. Kuperman, Sidney R. Nagel

Vibrations in a granular material can spontaneously produce convection rolls reminiscent of those seen in fluids. Magnetic resonance imaging provides a sensitive and noninvasive probe for the detection of these convection currents, which have otherwise been difficult to observe. A magnetic resonance imaging study of convection in a column of poppy seeds yielded data about the detailed shape of the convection rolls and the depth dependence of the convection velocity. The velocity was found to decrease exponentially with depth; a simple model for this behavior is presented here.

More than a century ago, Faraday discovered that vibration can produce large-scale convection within a granular medium (*1*). Like molecules of a liquid heated from below, grains in a vibrating container continuously circulate between the bottom and top of the container. This ubiquitous phenomenon has implications for a wide variety of industrial processes, but the mechanisms that cause it are poorly understood even today (*2*). One unusual and perplexing feature is that the grains flow rapidly at the container walls rather than exhibiting the nonslip boundary condition observed in normal fluids. Investigators have been hampered by an inability to see motion deep inside a container so as to determine the full, three-dimensional convection pattern. Here, we report a noninvasive convection measurement technique that provides the detailed shape of the boundary layer and the functional form of the convection velocity.

Much effort in the past has focused on calculations of flow patterns and velocity profiles in industrially important situations such as chute flow and discharge from hoppers (*3–5*). More recently, large-scale computer simulations have been used to model convection (*6, 7*) and size separation (*8, 9*) in vibrated granular materials, but few experimental data on the interior of the granular flow are available for comparison with these models. In two-dimensional geometries, particles can be tracked optically (*10–12*); however, because such experiments necessitate front and back walls and their associated friction, it is unclear how these results relate to the more technologically relevant three-dimensional case, where granular convection can be a driving mechanism for size segregation (*13*) and where optical tracking is difficult. Early three-dimensional experiments used invasive methods in which the granular aggregate was cast in resin and cross sections were cut and examined (*14*). Noninvasive techniques using x-rays (*15*) and radioactive tracer particles (*16*) also have been explored, but neither approach has yet resulted in a high-resolution tool for the study of granular flow.

Magnetic resonance imaging (MRI) offers a promising alternative for visualizing convection flows. With this technique it is possible to image arbitrary cross sections through the interior of a granular aggregate and to obtain direct information about the velocity profiles. Altobelli *et al.* (*17*) have used MRI to study particles in liquid suspensions, and Nakagawa *et al.* (*18*) have used MRI to study the flow of dry granular materials in a rotating drum. In the latter study, the use of oil-containing seeds as the granular material provided sufficient free protons in the liquid state to produce an acceptable signal-to-noise ratio. Here, we use this technique to study convection rolls induced by vertical vibrations in a column of white poppy seeds.

A magnetic resonance image of the poppy seeds at rest in a small cylindrical glass container is shown in Fig. 1. As in (*18*), a single layer of seeds was glued to the inner surface of the container. This coating makes the walls of the container visible in the image, thus giving a base line from which to measure the vertical displacement of the seeds, and it also provides a controlled degree of friction between the walls and the vibrating seeds (*13*). Inside the bore of the MRI magnet,

E. E. Ehrichs, H. M. Jaeger, J. B. Knight, S. R. Nagel, James Franck Institute and Department of Physics, University of Chicago, 5640 South Ellis Avenue, Chicago, IL 60637, USA.
G. S. Karczmar and V. Yu. Kuperman, Department of Radiology, University of Chicago, Chicago, IL 60637, USA.

*To whom correspondence should be addressed.

Downloaded from www.sciencemag.org on May 3, 2012